

Article

Research on Multi-Objective Process Parameter Optimization Method in Hard Turning Based on an Improved NSGA-II Algorithm

Zhengrui Zhang, Fei Wu * and Aonan Wu

School of Mechanical and Electronic Engineering, Wuhan University of Technology, Wuhan 430070, China; zhangzhengrui@whut.edu.cn (Z.Z.); wuaonan@whut.edu.cn (A.W.)

* Correspondence: wufei@whut.edu.cn; Tel.: +86-153-2737-8758

Abstract: To address the issue of local optima encountered during the multi-objective optimization process with the Non-dominated Sorting Genetic Algorithm II (NSGA-II) algorithm, this paper introduces an enhanced version of the NSGA-II. This improved NSGA-II incorporates polynomial and simulated binary crossover operators into the genetic algorithm's crossover phase to refine its performance. For evaluation purposes, the classic ZDT benchmark functions are employed. The findings reveal that the enhanced NSGA-II algorithm achieves higher convergence accuracy and surpasses the performance of the original NSGA-II algorithm. When applied to the machining of the high-hardness material 20MnCrTi, four algorithms were utilized: the improved NSGA-II, the conventional NSGA-II, NSGA-III, and MOEA/D. The experimental outcomes show that the improved NSGA-II algorithm delivers a more optimal combination of process parameters, effectively enhancing the workpiece's surface roughness and material removal rate. This leads to a significant improvement in the machining quality of the workpiece surface, demonstrating the superiority of the improved algorithm in optimizing machining processes.

Keywords: multi-objective optimization; hard turning; NSGA-II algorithm; improved algorithm; process parameters; machining process



Citation: Zhang, Z.; Wu, F.; Wu, A. Research on Multi-Objective Process Parameter Optimization Method in Hard Turning Based on an Improved NSGA-II Algorithm. *Processes* **2024**, *12*, 950. <https://doi.org/10.3390/pr12050950>

Received: 10 April 2024

Revised: 28 April 2024

Accepted: 4 May 2024

Published: 7 May 2024



Copyright: © 2024 by the authors. Licensee MDPI, Basel, Switzerland. This article is an open access article distributed under the terms and conditions of the Creative Commons Attribution (CC BY) license (<https://creativecommons.org/licenses/by/4.0/>).

1. Introduction

With the advancement of manufacturing technologies, intelligent neural networks have increasingly been integrated into the machining of high-hardness materials [1,2] and the optimization of multi-objective process parameters [3–5]. As the complexity of workpieces escalates and process requirements become more stringent, optimizing for a single objective is no longer feasible. Instead, an optimal combination of process parameters is determined through algorithms and experimental procedures to machine the workpieces [6–8]. This approach not only ensures the quality of the machined workpiece but also enhances processing efficiency and reduces production costs, aligning with the evolving demands of modern manufacturing practices.

Hard turning is a process that typically involves machining workpieces with hardness exceeding 50 HRC (Rockwell C scale). For this application, cutting tools fabricated from high-hardness materials, such as Cubic Boron Nitride (CBN) and Polycrystalline Cubic Boron Nitride (PCBN), are commonly selected [9–11]. These materials are not only characterized by their exceptional hardness but also demonstrate superior thermal conductivity and wear resistance [12,13], providing a significant advantage in machining high-hardness materials [14]. The optimization of machining parameters for such materials [15,16] presents a critical technical challenge that is essential for enhancing the efficiency of turning processes and ensuring superior workpiece surface quality.

In recent years, extensive research has been conducted on the incorporation of multiple decision variables into the turning process. This approach acknowledges that considering

multiple factors can improve the precision and persuasiveness of the objectives, leading to the emergence of multi-objective optimization problems as a prevalent research topic [17]. Commonly employed optimization algorithms include “the Non-dominated Sorting Genetic Algorithm II” (NSGA-II) [18–22], “the Multi-Objective Evolutionary Algorithm based on Decomposition” (MOEA/D) [23], “the Response Surface Methodology (RSM) algorithm” [24], and “the Strength Pareto Evolutionary Algorithm 2” (SPEA2) [25]. NSGA-II evolved from the original NSGA [26], which used a non-dominated sorting method for multi-objective problems. NSGA-II [27] introduced an elitist strategy to reduce computational complexities. With increasing optimization challenges, especially in higher-dimensional spaces, NSGA-III [28] was developed, incorporating a reference point-based method to enhance diversity and performance. Some researchers have improved NSGA-II or NSGA-III to obtain the so-called NSGA-IV [29], which further improves their efficiency and effectiveness in complex optimization scenarios.

These algorithms are adept at addressing multi-objective optimization challenges and have significantly contributed to advancements in this field. NSGA-II stands out because of its superior performance compared to simpler algorithms and higher computational efficiency compared to more complex algorithms, and is widely recognized in both academia and industry. These advantages make it particularly suitable for practical engineering applications, so we choose it as the benchmark algorithm in this study to avoid the complexity of the algorithm and the waste of computing resources. However, a recurring issue with these optimization algorithms is the uneven convergence of the population and a propensity to become trapped in local optima, which can impact the outcomes of multi-objective optimizations [30]. Thus, further analysis and enhancements of these algorithms are necessary to overcome this challenge.

To address the issue at hand, this paper introduces an enhancement to the NSGA-II algorithm by integrating a crossover-mutation hybrid strategy into its crossover process. This modification significantly improves convergence and distribution. The improved NSGA-II algorithm is applied to the multi-objective optimization problem of machining parameters for the external cylindrical turning of carburized steel 20MnCrTi, known for its high hardness. The results showcase the enhanced algorithm’s superior convergence accuracy and expedited convergence rate, leading to optimization solutions that more closely approximate the global optimum. Such improvements render the algorithm notably more effective in solving multi-objective optimization problems related to cutting parameters.

This paper is organized as follows. Section 1 outlines the research motivation by discussing the state and challenges in hard turning processes. Section 2 introduces the concept of multi-objective optimization. Section 3 elaborates on enhancements made to the NSGA-II algorithm for better machining guidance. Section 4 assesses the modified algorithm’s performance through ZDT series test functions. Section 5 compares the improved NSGA-II with traditional NSGA-II, NSGA-III and MOEA/D, and theoretically proves that the improved NSGA-II has better performance. Section 6 reports the experimental verification of the four algorithms, and the experimental results prove the practical significance of the proposed method. Section 7 concludes with a summary of the research findings.

2. Multi-Objective Optimization Problems

In multi-objective optimization, models are optimized across multiple objectives. It is not feasible to achieve the optimal outcome for every objective function independently; rather, it is necessary to consider the interplay among various objective factors, which requires assigning specific weights to each objective function. In tackling such problems, the goal is to derive a set of solutions, rather than a singular optimal solution. These solutions are known as Pareto-optimal solutions [31]. With the development of genetic algorithms, the challenge of being ensnared in local optima within multi-objective optimization contexts has been mitigated, thereby ensuring global search capabilities and maintaining population diversity.

2.1. Multi-Objective Optimization Mathematical Expressions

Generally, when tackling such problems, the optimization objective functions mostly aim to minimize their values for computational convenience [32]. Therefore, the mathematical description of multi-objective problems is as shown in Equation (1):

$$\begin{aligned} \min\{F(x)\} &= [f_1(x), f_2(x), \dots, f_m(x)] \\ \text{Subject_to : } &\begin{cases} g_i(x) \geq 0, i = 1, 2, \dots, k \\ h_j(x) = 0, j = 1, 2, \dots, l \end{cases} \end{aligned} \quad (1)$$

In the above equation, $F(x)$ represents the objectives to be optimized in multi-objective optimization problems, and the space in which these objectives exist is known as the objective space. x is a vector in an n -dimensional space, denoted as R^n , and the space in which x resides constitutes the decision space of the multi-objective optimization problem. The constraints are defined as $h_j(x) = 0, j = 1, 2, \dots, l, g_i(x) \leq 0, i = 1, 2, \dots$.

2.2. Pareto-Optimal Solutions in Multi-Objective Optimization

For two variables $a, b \in X$, assuming $a > b$, if and only if:

$$\{\forall i \in \{1, 2, \dots, n\} f_i(a) \leq f_i(b)\} \wedge \{\exists j \in \{1, 2, \dots, n\} f_j(a) < f_j(b)\} \quad (2)$$

For a given variable a , it is considered a non-dominated solution, or a Pareto-optimal solution, if there are no other variables within the decision variable set that dominate a . Within this context, should there exist a variable X within the decision variable set, and for any variable S , the condition $F(X) \leq F(S)$ holds for a given objective function F , then S is designated as an optimal solution, also known as a non-inferior solution, in relation to the objective functions. In the realm of multi-objective optimization problems, it is noteworthy that non-inferior solutions are not singular; rather, there exists a plurality of such solutions. The aggregate of all non-inferior solutions is termed the Pareto Front, representing a critical concept in multi-objective optimization analysis.

As illustrated in Figure 1, the multi-objective optimization problem is simplified into a bi-objective optimization problem involving the optimization of objective functions $f_1(x)$ and $f_2(x)$. The goal is to identify a set of solutions that minimize these objective functions, satisfying Equation (1). The Pareto-optimal solutions in the context of multi-objective optimization problems comprise a suite of solutions, each characterized by the property that any improvement in one objective necessitates the degradation of at least one other objective. These solutions are interdependent and non-dominant, collectively constituting an optimal set of solutions. For example, within this set, points A and B are positioned on the Pareto Front, signifying their optimality, whereas point C is suboptimal as it is dominated by both points A and B.

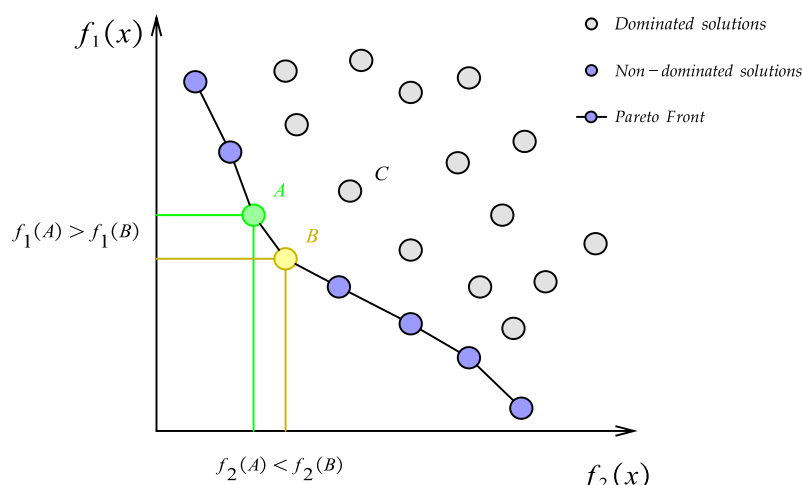


Figure 1. Pareto Front graphical representation.

3. Improvement and Implementation of NSGA-II Algorithm Analysis

3.1. Analysis of the NSGA-II Algorithm

The NSGA-II algorithm (Nondominated Sorting Genetic Algorithm II), developed by Deb et al. [27], stands as a prominent multi-objective genetic algorithm. This sophisticated algorithm stratifies the population into distinct levels based on the principle of dominance, effectively eliminating individuals of lesser dominance to foster both diversity and uniformity within the population. The NSGA-II algorithm is structured around four core components: the selection of the population, the mechanisms of crossover and mutation, the implementation of fast non-dominated sorting, the calculation of crowding distance, and the integration of elitism, each contributing to its efficiency and effectiveness in solving multi-objective optimization problems.

The processes of selection, crossover, and mutation within populations are inspired by the evolutionary genetic mechanisms observed in natural species, designed to foster the generation of new individuals and augment the algorithm's search efficacy. The NSGA-II algorithm employs the Simulated Binary Crossover (SBX) [33] operator and the Polynomial Mutation (PM) [34] operator, which are rigorously defined by the Equations (3) and (4), respectively. These operators are instrumental in mimicking natural genetic variations, thereby enhancing the diversity and exploratory power of the algorithm in navigating complex multi-objective optimization landscapes.

$$\beta = \begin{cases} (2u_i)^{\frac{1}{\eta+1}}, & u_i \leq 0.5 \\ \frac{1}{[2(1-u_i)]^{\frac{1}{\eta+1}}}, & u_i \geq 0.5 \end{cases} \quad (3)$$

$$\delta = \begin{cases} (2r_k)^{\frac{1}{\eta_m+1}}, & r_k \leq 0.5 \\ 1 - [2(1 - r_k)]^{\frac{1}{\eta_m+1}}, & r_k \geq 0.5 \end{cases} \quad (4)$$

In Equation (3), u_i denotes a random variable uniformly distributed across the interval $[0,1]$, while η , the crossover distribution index, typically spans a range between 20 and 30. The chosen value for η plays a critical role in dictating the dispersion of offspring relative to their parental genes. Analogously, Equation (4) introduces r_k as another random variable uniformly distributed over $[0,1]$, with η_m signifying the mutation distribution index, which influences the mutation process's granularity.

The fast non-dominated sorting, based on Pareto dominance, categorizes solutions using multiple objective functions $f_i(x)$ where i ranges from 1 to k . An individual x_1 dominates x_2 if $f_i(x_1) < f_i(x_2)$ for all objectives, and weakly dominates if $f_i(x_1) \leq f_i(x_2)$ with at least one strict inequality. The sorting process involves assigning a non-dominated rank starting from individuals with a dominance count of zero. Successive ranks are assigned by decrementing the dominance count and re-evaluating until all individuals are ranked. As depicted in Figure 2, diverse shapes symbolize different Pareto ranks, with circles specifically denoting the most optimal tier of solutions. This visual representation facilitates a clear understanding of the hierarchical nature of solution ranks within the Pareto Front.

The crowding distance calculation plays a pivotal role in situations where two individuals are of the same rank, by giving preference to the individual that exhibits a greater crowding distance. This distance is determined through calculations of mutual crowding among individuals. To calculate the crowding distance for individuals within a given rank, define m as the total number of individuals, each labeled x_i for $i = 1$ to m . The individuals x_{i-1} and x_{i+1} are the adjacent members in the sequence. With n objective functions, where $f_{(min)n}$ and $f_{(max)n}$ are the minimum and maximum values for the n th function, the crowding distance y_i for each individual starts at zero. Crowding distances are computed using the methodology outlined in Equation (5).

$$y_i = (x_{i+1} - x_{i-1}) / (f_{(max)n} - f_{(min)n}) \quad (5)$$

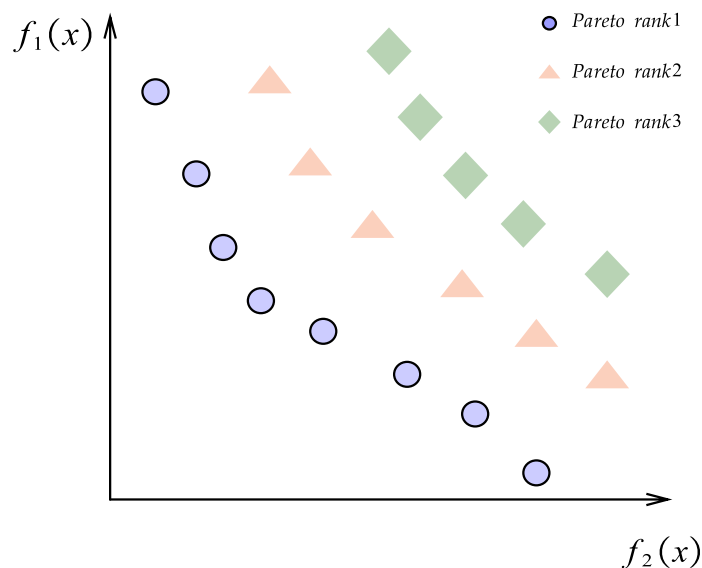


Figure 2. Pareto-optimal solutions.

As illustrated in Figure 3, the concept of crowding distance can be effectively visualized using rectangular diagrams, which aid in comprehending the spatial differences among individuals within the same rank. This method ensures diversity among the selected solutions by maintaining a spread of individuals across the solution space.

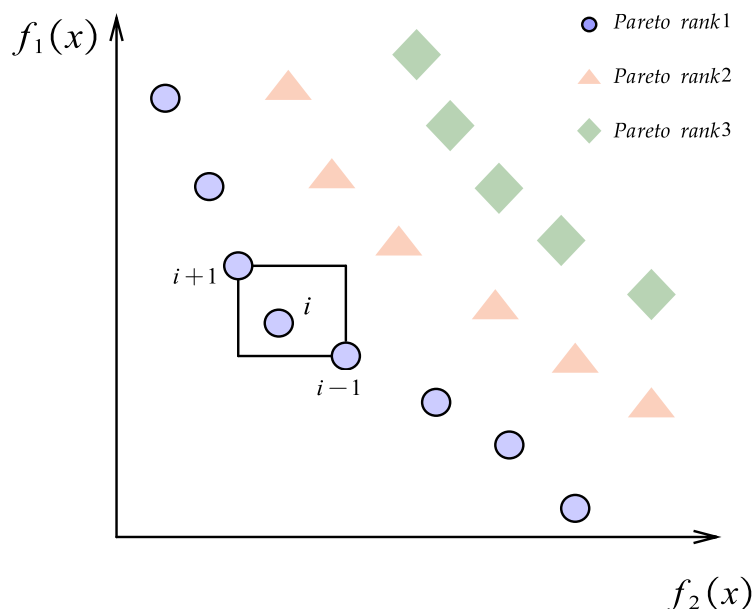


Figure 3. Crowding-distance calculation.

The elitism strategy is characterized by a selective culling process within the hierarchically arranged solution sets, favoring the retention of individuals that not only possess superior ranks but also exhibit extensive crowding distances. As demonstrated in Figure 4, the parent population (P) and the offspring population (C) are combined and subjected to a fast non-dominated sorting process, resulting in six Pareto ranks. Subsequently, the new parent population is generated by iteratively adding individuals from each rank in ascending order until the required population size is reached. When adding individuals from the $(k + 1)$ -th rank, if only a subset of individuals is needed to meet the desired population size, those individuals are further sorted based on their crowding distance in descending order. The required individuals are then selected, and the remaining individuals from the

$(k + 1)$ -th rank, as well as all subsequent ranks, are discarded. In Figure 4, this crowding distance sorting occurs at the third Pareto rank. This strategy underscores the algorithm's commitment to preserving excellence and diversity within the evolving populations.

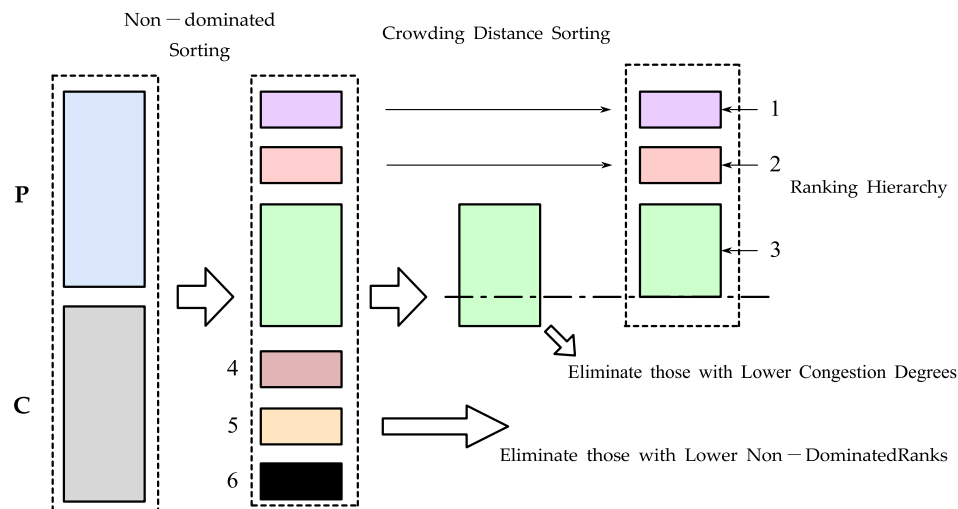


Figure 4. Execution steps of the elitism preservation strategy.

3.2. Improvement of the NSGA-II Algorithm

The improved NSGA-II algorithm is mainly an improvement of the crossover phase of the genetic algorithm. It combines simulated binary crossover and polynomial mutation. Suppose x_1 and x_2 represent the individuals undergoing the crossover, with V denoting the problem's dimension, which corresponds to the number of genes. x_1^j and x_2^j represent the j -th gene of these two individuals. The resulting offspring, denoted as y_1 and y_2 , are characterized by y_1^j and y_2^j , which signify the j -th gene of the offspring. The steps for generating offspring are as follows:

Step 1: Generate a random number at random, $r(j) \in (0, 1)$

Step 2: Calculate the value of $\beta(j)$:

$$\beta(j) = \begin{cases} (2r(j))^{\frac{1}{\eta_c+1}}, & r(j) \leq 0.5 \\ 1 - (2 \cdot (1 - r(j)))^{\frac{1}{\eta_c+1}}, & r(j) > 0.5 \end{cases} \quad (6)$$

Step 3: Calculate the values of y_1^j, y_2^j :

$$\begin{aligned} y_1^j &= \frac{(1+\beta(j)) \cdot x_1^j + (1-\beta(j)) \cdot x_2^j}{2} \\ y_2^j &= \frac{(1-\beta(j)) \cdot x_1^j + (1+\beta(j)) \cdot x_2^j}{2} \end{aligned} \quad (7)$$

Step 4: Judge whether y_1^j, y_2^j cross the boundary. If so, take the boundary value.

The η_c above is a self-defined non-negative real number called the cross-distribution index, where the larger η_c is, the closer the resulting individual is to the parent individual, and the smaller η_c is, the further away it is from the parent. This means that the larger η_c is, the smaller the area to be searched, and vice versa.

3.3. Implementation of the NSGA-II Algorithm

The pivotal workflow of the enhanced NSGA-II algorithm is depicted in Figure 5, with the implementation procedure detailed as follows:

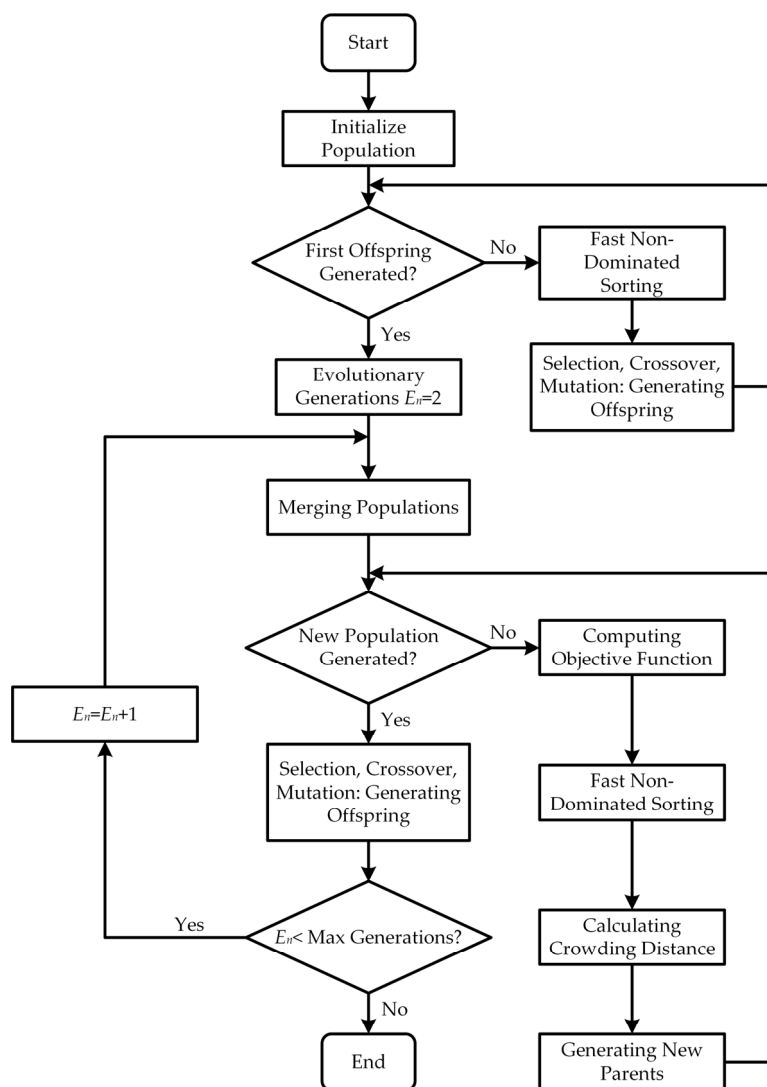


Figure 5. Algorithm flow chart.

Step 1: Initialize the population;

Step 2: Evaluate whether to generate the inaugural subpopulation. If yes, set the evolutionary generation, denoted as E_n , to 2 and advance to the subsequent step. In the negative case, apply methodologies such as fast non-dominated sorting on the initial population to yield the progeny population;

Step 3: Amalgamate the progenitor and progeny populations to formulate a novel population ensemble;

Step 4: Evaluate whether a new progenitor population has been created. If yes, execute a selective cross-mutation operation on the newly constituted progenitor population. Conversely, employ strategies such as fast non-dominated sorting to conceive a fresh progenitor population;

Step 5: Ascertain if the evolutionary generation E_n is inferior to the maximum evolutionary threshold. Should this be the case, increment the evolutionary generation E_n by 1 and loop back to the third step, persisting until the cycle concludes. If not, proceed to the algorithm's end.

This segment addresses the domain of multi-objective optimization with constraints, incorporating specific limitations within the programmatic framework. NSGA-II is suitable for solving multi-objective optimization problems with up to three dimensions, meaning that the number of optimization objectives does not exceed 3.

4. Algorithm Performance Testing and Analysis

The classical ZDT function family [35] is employed as a set of test functions to assess the NSGA-II algorithm before and after improvement under a consistent evaluation system.

4.1. Metrics for Evaluating Algorithm Performance

In evaluating the enhancements brought to the NSGA-II algorithm in this research, two key metrics are utilized: the Generational Distance (GD) as the distance metric, and Spacing (SP) as the distribution metric. The Generational Distance (GD) metric is instrumental in gauging the algorithm's convergence capabilities [20], with its computational formula presented as Equation (8).

$$GD = \frac{\left(\sum_{i=1}^a x_i^q \right)^{1/q}}{a} \quad (8)$$

In Equation (8), two parameters are defined: GD_k and GD_t . Where a represents the number of vectors in GD_k , q is set to 2, and x_i denotes the Euclidean distance between each one-dimensional vector in the target space and the nearest corresponding vector in GD_t . A result of 0 indicates $GD_t = GD_k$, while a non-zero result signifies the degree to which GD_k deviates from GD_t , with smaller deviations being preferable.

SP (Spacing) is the most commonly used distribution metric [36]. Its calculation formula is shown in Equation (9):

$$SP(A) = \sqrt{\frac{1}{N-1} \sum_{i=1}^N (\bar{d} - d_1(a_i, A/a_i))^2} \quad (9)$$

In the formula above, d represents the average of all $d_1(a_1, A/a_1)$, $d_1(a_2, A/a_2)$, ..., $d_N(a_N, A/a_N)$ and $d_i(a_i, A/a_i)$, where a_i is the solution's L1-norm distance from the set A/a_i , calculated as in Equation (10):

$$d_1(a_i, A/a_i) = \min_{a \in A/a_i} \sum_{j=1}^m |a_{ij} - a_j| \quad (10)$$

In this equation, m signifies the number of objectives, and a_{ij} represents the j -th objective for solution a_i . Lower SP values indicate better uniformity.

4.2. Performance Testing of Algorithms and Analysis of Results

To evaluate the performance of the algorithms both pre- and post-enhancement, this study subjects the two algorithmic variants to analysis under consistent parameter configurations. These parameters include a population size set at 150, a cap of 500 iterations, a crossover probability fixed at 0.8, and a mutation probability also at 0.8. For each set of test functions, the algorithms underwent five independent trials, ensuring a robust assessment of their performance and reliability across varying scenarios.

The examination of the data showcased in Figures 6–10, particularly when comparing the convergence trends of the distance and distribution metrics across the quintet of test function sets, reveals a notable performance enhancement in the modified NSGA-II algorithm. It exhibits expedited convergence, augmented convergence efficacy, and a more even solution distribution relative to its predecessor, the conventional NSGA-II algorithm. These outcomes are indicative of the significant performance boost conferred by the integration of a hybrid operator that melds the simulated binary and polynomial mechanisms. Consequently, this amalgamation in the enhanced NSGA-II algorithm not only elevates its convergence efficiency but also refines its distribution attributes, highlighting its advanced optimization capabilities.

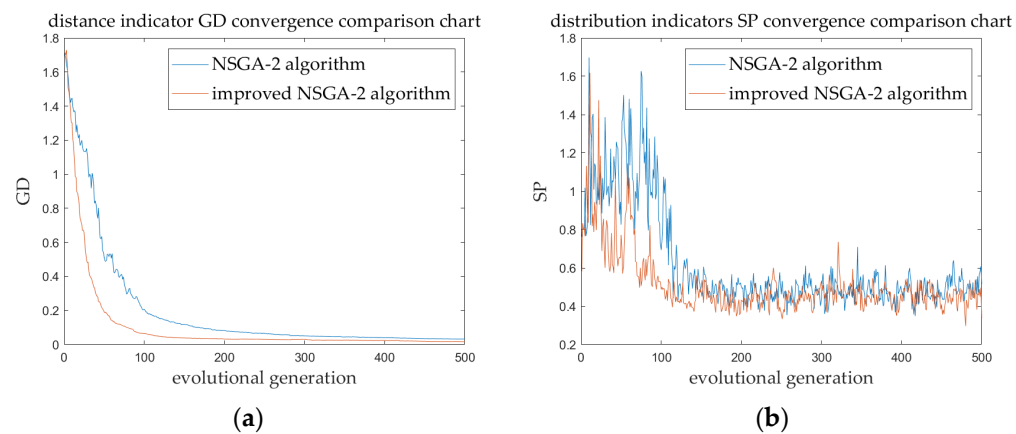


Figure 6. Convergence of generational distance and spacing of ZDT1 function. (a) Convergence comparison of distance index. (b) Convergence comparison of distribution index.

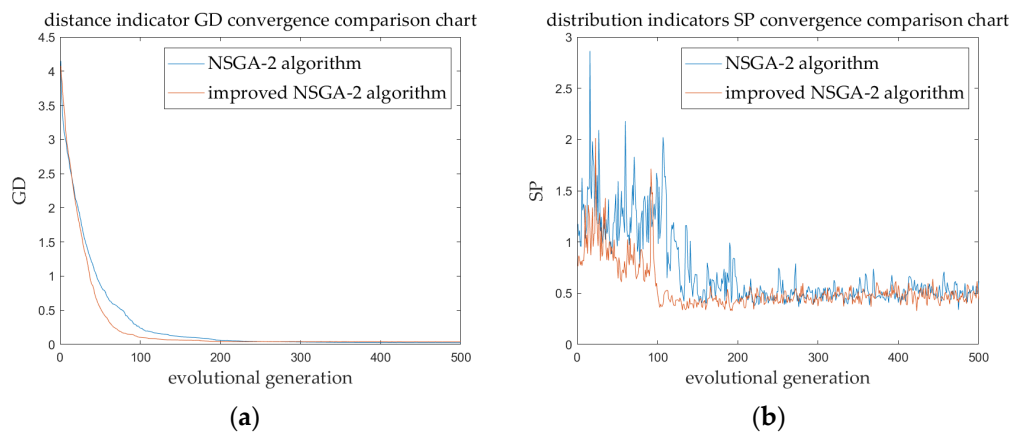


Figure 7. Convergence of generational distance and spacing of ZDT2 function. (a) Convergence comparison of distance index. (b) Convergence comparison of distribution index.

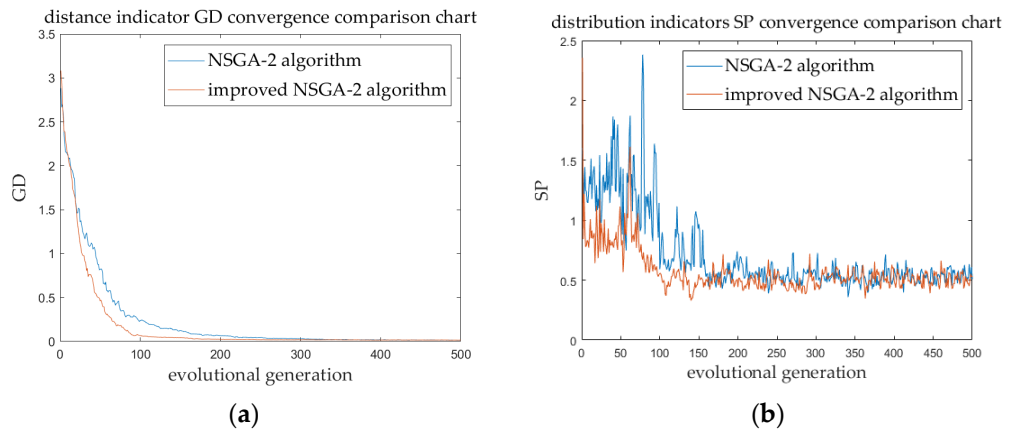


Figure 8. Convergence of generational distance and spacing of ZDT3 function. (a) Convergence comparison of distance index. (b) Convergence comparison of distribution index.

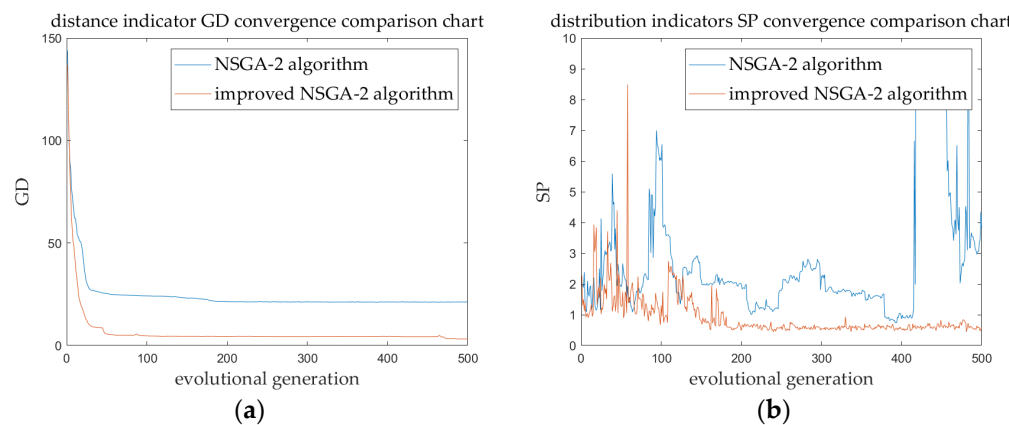


Figure 9. Convergence of generational distance and spacing of ZDT4 function. (a) Convergence comparison of distance index. (b) Convergence comparison of distribution index.

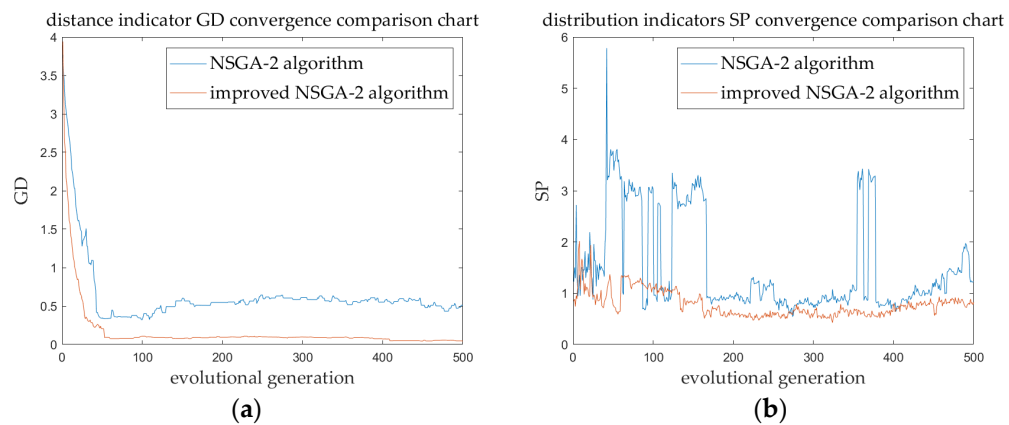


Figure 10. Convergence of generational distance and spacing of ZDT6 function. (a) Convergence comparison of distance index. (b) Convergence comparison of distribution index.

5. Comparative Analysis of the Algorithmic Models

5.1. Development of a Bi-Objective Optimization Model

The working life and performance of mechanical components are related to the material, heat treatment, surface microgeometry, and surface roughness of the components. Surface roughness affects various aspects of component performance, including wear resistance, sealing, fatigue strength, among others. In this study, a non-linear regression equation is established for the relationship between surface roughness R_a and cutting parameters. The prediction model is represented in Equation (11):

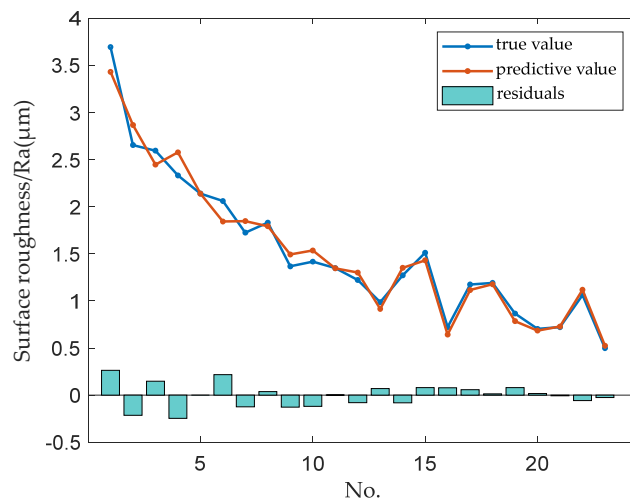
$$R_a = a_0 + a_1 \cdot \sqrt{n} + a_2 \cdot f + a_3 \cdot a_p + a_4 \cdot f^2 + a_5 \cdot n \cdot a_p \quad (11)$$

In Equation (11), R_a denotes the surface roughness (μm), n stand for the spindle speed (mm/r), f represents the feed rate (mm/min), a_p is the cutting depth (mm), and a_0, a_1, a_2, a_3, a_4 and a_5 are constants. Surface roughness measurements of the workpiece were conducted using a TR210 surface roughness measuring instrument with a sampling length of 60 mm. To minimize errors, measurements were taken at different positions on the workpiece by rotating it to five different angles. The average of these five measurements was used as the final result. The data from 23 sets obtained through orthogonal tests are presented in Table 1.

Table 1. Twenty-three (23) sets of data results of orthogonal test.

No.	Spindle Speed/(r/min)	Feed Rate/(mm/min)	Cutting Depth/(mm)	Surface Roughness/Ra (μm)					Average Roughness/(\mathbf{\mu}\text{m})
				Ra ₁	Ra ₂	Ra ₃	Ra ₄	Ra ₅	
1	300	20	0.1	3.317	4.680	3.833	3.087	3.546	3.6926
2	300	25	0.2	2.561	2.520	2.777	2.583	2.825	2.6532
3	300	30	0.3	2.961	2.470	1.956	2.706	2.875	2.5936
4	350	25	0.2	1.988	2.630	2.103	2.052	2.882	2.3310
5	350	30	0.3	2.927	2.245	1.488	2.242	1.791	2.1386
6	350	35	0.4	0.455	3.372	2.441	3.573	0.457	2.0596
7	400	30	0.3	0.952	1.489	2.251	2.282	1.648	1.7244
8	400	35	0.2	2.413	1.148	2.215	2.069	1.309	1.8308
9	400	40	0.4	1.250	1.330	1.502	1.531	1.220	1.3666
10	450	35	0.2	1.208	1.525	1.527	1.518	1.304	1.4164
11	450	40	0.3	1.198	1.304	1.042	1.323	1.472	1.3478
12	450	45	0.4	1.016	1.119	1.417	1.642	0.915	1.2218
13	500	40	0.4	1.079	0.832	0.763	1.171	1.086	0.9862
14	500	45	0.2	1.512	1.236	1.404	1.157	1.341	1.2710
15	500	50	0.3	1.462	1.593	1.472	1.432	1.595	1.5108
16	550	40	0.4	0.650	0.726	0.777	0.671	0.785	0.7218
17	550	45	0.2	1.585	1.058	1.054	1.076	1.097	1.1740
18	550	50	0.3	1.122	1.236	1.487	1.089	1.021	1.1910
19	600	40	0.2	0.921	0.900	0.800	0.781	0.931	0.8666
20	600	45	0.3	0.693	0.721	0.844	0.763	0.594	0.7030
21	600	50	0.4	0.964	0.434	1.284	0.526	0.401	0.7218
22	600	55	0.4	0.490	0.451	1.836	1.260	1.271	1.0616
23	600	50	0.5	0.390	0.410	0.848	0.437	0.412	0.4994

The dataset from Table 1 was imported into the MATLAB R2022a toolbox to deduce the surface roughness expression via non-linear regression model analysis. Figure 11 depicts the variation curves for experimental and predicted values, represented by blue and orange lines, respectively. Below these curves, the bar chart displays the residuals for corresponding ordinal numbers, detailing the discrepancies between the experimental and predicted data. The horizontal axis represents the experimental number, corresponding to the “No.” column in Table 1; the vertical axis denotes the surface roughness (Ra) measured in micrometers (μm). An examination of Figure 11 indicates that with an increase in spindle speed, the surface roughness value tends to stabilize, exhibiting fluctuations within a narrow band of 1. The absolute residuals between the forecasted and actual experimental surface roughness values are confined within the range of (0, 0.3), suggesting a commendably low error margin of under 10%.

**Figure 11.** Surface roughness fitting function.

One of the crucial indicators for assessing cutting efficiency is the MRR (material removal rate) [37], which represents the volume of material removed per unit of time.

The optimization objectives involve reducing production cycles and minimizing costs. Therefore, to enhance the material removal rate, cutting speed, feed rate, and cutting depth should be increased to the maximum extent possible. The formula for the material removal rate is presented in Equation (12):

$$MRR = v_c \cdot f \cdot a_p \quad (12)$$

In Equation (12), v_c represents the cutting speed, and its calculation as follows:

$$v_c = \frac{\pi \cdot d \cdot n}{1000} \quad (13)$$

In Equation (13), d denotes the workpiece's rotational diameter, measured in millimeters. Upon substituting this value into the equation, we can derive the result:

$$MRR = \frac{\pi \cdot d \cdot n \cdot f \cdot a_p}{1000} \quad (14)$$

Experimental data from Table 1 were processed using MATLAB R2022a software to derive the regression equation. The mathematical statistical model for surface roughness is established as shown in Equation (15):

$$Ra = 9.9945 - 0.1821 \cdot \sqrt{n} - 0.2233 \cdot f + 0.1775 \cdot a_p + 0.0029 \cdot f^2 - 0.0037 \cdot n \cdot a_p \quad (15)$$

By integrating the insights from Equation (15) and the material removal rate formula outlined in Equation (12), we derive the formulation for the objective function along with the constraint distribution for the decision variables, as depicted in Equation (16). Given the preference for a higher material removal rate and a lower surface roughness, a negative sign is introduced before the material removal rate in the objective function formulation. This implies that a lower value of $-MRR$ corresponds to a higher material removal rate, thereby fostering uniformity within the solution set and aligning with the optimization goals.

$$\begin{aligned} \text{objective function : } & \left\{ \begin{array}{l} \min Ra = 9.9945 - 0.1821 \cdot \sqrt{n} - 0.2233 \cdot f + 0.1775 \cdot a_p \\ \quad + 0.0029 \cdot f^2 - 0.0037 \cdot n \cdot a_p \\ \min (-MRR) = (\pi \cdot d \cdot n \cdot f \cdot a_p) / 1000 \end{array} \right. \\ \text{constraint distribution : } & \left\{ \begin{array}{l} 500r/min \leq n \leq 600r/min \\ 30mm/min \leq f \leq 60mm/min \\ 0.2mm \leq a_p \leq 0.5mm \end{array} \right. \end{aligned} \quad (16)$$

5.2. Analyzing the Results of Comparing Algorithms

In this section, the improved NSGA-II algorithm is compared with three other multi-objective algorithms: MOEA/D, NSGA-III, and the original NSGA-II. Each algorithm is employed to solve the multi-objective optimization problem of external cylindrical turning parameters for high-hardness material carburized steel 20MnCrTi. To ensure fairness, this study uses uniform parameter settings to evaluate the performance of the algorithms. These parameters encompassed a population size of 150, a maximum of 500 iterations, a crossover probability set at 0.8, and a mutation probability also at 0.8. Each of the algorithm was independently tested five times for each set of test functions. Figure 12 presents a comparison of the Pareto solutions obtained using the improved NSGA-II algorithm, the traditional NSGA-II algorithm, MOEA/D, and NSGA-III algorithms. This comparison aims to highlight the enhancements in solution distribution and optimization efficiency achieved through the algorithmic improvements.

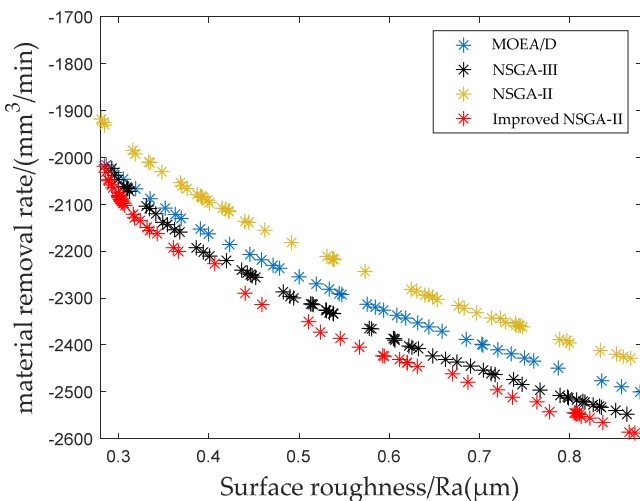


Figure 12. Different algorithms' Pareto solutions comparison figure.

The analysis of Figure 12 clearly demonstrates that the optimized NSGA-II algorithm delivers a relatively uniform and continuous distribution of optimal solutions across the specified region, showcasing enhanced convergence efficiency compared to the other three algorithms. Notably, the optimized algorithm achieves lower surface roughness values while maintaining equivalent material removal rates, indicating its ability to produce smoother workpiece surfaces without compromising machining productivity. Additionally, with comparable surface roughness levels, the optimized NSGA-II algorithm facilitates higher material removal rates than the other three algorithms, underscoring its superior performance.

Further examination of Figure 12 indicates that solutions positioned in the lower-right quadrant are characterized by higher surface roughness and greater material removal rates, while those in the upper-left quadrant correspond to lower surface roughness and reduced material removal rates. This trend suggests a positive correlation between material removal rates and surface roughness, wherein an increase in one leads to a rise in the other, and vice versa. Given the machining requirements for workpieces, the optimal solution set derived from the model optimization is deemed both logical and viable.

Using the improved NSGA-II algorithm to select five optimal solution sets with an order of 1 from the Pareto-optimal solution set, the experimental results from Table 2's improved NSGA-II algorithm reveal that the first set, compared to other sets with the same rank order of 1, has a crowding distance of 0.0700, which is higher than that of the other groups. Therefore, the first set represents the best combination of process parameters after 500 iterations. Specifically, this combination entails a surface roughness of 0.2843 μm and a material removal rate of 1889.4 mm^3/min . Additionally, we utilized the same methodology to determine the optimal process parameter combinations using the traditional NSGA-II algorithm, MOEA/D algorithm, and NSGA-III algorithm. Four sets of process parameter combinations derived from these four algorithms were then used to conduct turning experiments on the workpieces, which further proves the advantages of the improved NSGA-II algorithm.

Table 2. Improved NSGA-II algorithm with partial Pareto-optimal solutions.

No.	Spindle Speed (r/min)	Feed Rate (mm/min)	Cutting Depth (mm)	Surface Roughness (mm)	Material Removal Rate (mm^3/min)	Order	Congestion Degree
1	590.1128	40.7663	0.5	0.2843	1889.4	1	0.0700
2	589.8763	41.6376	0.5	0.2993	1929.0	1	0.0694
3	590.0832	46.3484	0.5	0.4482	2148.0	1	0.0603
4	589.9995	46.7531	0.5	0.4676	2166.5	1	0.0593
5	596.2747	38.5372	0.5	0.5255	1804.7	1	0.0571

6. Example Analysis of High Hardness Materials

The optimization experiment for machining parameters of high-hardness materials was carried out on an SK50P CNC (Computer Numerical Control) horizontal turning machine, as depicted in Figure 13. This versatile machine tool is well-suited for various sectors, including the light industry, shipbuilding, and machinery manufacturing. It features a spindle speed range from 21 to 1620 rpm, accommodating a maximum cutting diameter of 500 mm and a maximum cutting length of 820 mm. The machine's two-axis movement allows for a travel of 300 mm in the X direction and 850 mm in the Z direction, facilitating precision machining across a broad spectrum of applications. Table 3 lists the detailed parameters.



Figure 13. SK50P machine tool.

Table 3. SK50P machine tool performance parameters.

Spindle Speed/(r/min)	Machining Accuracy/(\mu m)	Maximum Cutting Diameter/(mm)	Maximum Cutting Length/(mm)	Two-Axis Travel/(mm)
21~1620	1.6	500	820	X:300 Z:850

6.1. The Experimental Scheme and Evaluation Indicators

In this experiment, the workpiece utilized is 20MnCrTi carburized steel, featuring a diameter of $\varphi 50$ mm and a length of 500 mm. This material has been subjected to heat treatment, achieving a substantial hardness of 55HRC. Table 4 lists the chemical components and Table 5 lists the main performance. The cutting tool employed is fabricated from Polycrystalline Cubic Boron Nitride (PCBN), with a cemented carbide base. Table 6 lists its physical characteristics. The tool's model is CNGA120408, distinguished by a tip radius of 0.8 mm. The tool holder used is the MCLNR2020K12 model. Figure 14 showcases both the workpiece and the cutting tool. The process parameter combinations applied in this study were determined through orthogonal experimental designs [38] and analysis using the four algorithms compared above. Table 7 outlines these parameter combinations, and group 9 was identified as the optimal set using the improved NSGA-II algorithm because it ranked on the non-dominated front with the highest crowding distance among the Pareto-optimal solutions. Groups 10 to 12 are the combination of process parameters obtained by the traditional NSGA-II algorithm, NSGA-III algorithm and MOEA/D algorithm, respectively.

Table 4. The 20MnCrTi chemical composition (mass fraction/%).

Designation	C	Si	Mn	Cr	S	P	Ti
20MnCrTi	0.17~0.23	0.17~0.37	0.80~1.10	1.00~1.30	≤ 0.03	≤ 0.03	0.04~0.10

Table 5. The 20MnCrTi main performance.

Designation	Tensile Strength/(Mpa)	Yield Strength/(Mpa)	Elongation/(%)	Section Shrinkage/(%)	Impact Work/(J)	Impact Toughness/(J/cm ²)	Hardness/(HRC)
20MnCrTi	≥1080	≥835	≥10	≥45	≥55	≥69	≥55

Table 6. Physical properties of PCBN tools.

Designation	Young's Modulus/(Gpa)	Thermal Conductivity/(W/m·K)	Poisson's Ratio	Density/(g/cm ³)	Specific Heat/(J/kg·°C)
PCBN	690	120	0.2	3.8	700



(a) PCBN tool



(b) PCBN tool and tool arbor



(c) φ50 mm×500 mm workpiece



(d) actual processing

Figure 14. PCBN tool and 20MnCrTi workpiece.**Table 7.** Table of horizontal factors of orthogonal test.

No.	Spindle Speed (r/min)	Unilateral Cutting Depth (mm)	Feed Rate (mm/min)
1	500	0.10	30
2	500	0.30	50
3	500	0.40	55
4	550	0.20	45
5	550	0.30	50
6	600	0.20	40
7	600	0.40	50
8	600	0.50	60
9	590	0.50	41
10	600	0.40	40
11	593	0.50	57
12	557	0.45	55

In Section 5.1, the study employs surface roughness, material removal rate, and workpiece machining state as the principal metrics for evaluation. Surface roughness serves as an indicator of workpiece surface quality, with lower values denoting superior surface

integrity. The material removal rate is utilized as a measure of machining efficiency, where higher rates signify enhanced efficiency. The machining state, classified into stable, transitional, and chatter phases, serves as a metric for assessing the stability of the machining process. The classification criteria for these states are not a focal point of this research. However, Table 8 still gives the division of processing stages of cylindrical hard turning.

Table 8. Hard turning chatter machining stage division.

No.	Processing Stages	Surface Roughness/Ra(μm)	Vibration Condition	Processing Noise
1	Stable	$R_a < 0.6$	No vibration	Noiseless
2	Transition	$0.6 \leq R_a < 1.0$	Slight vibration	Sharp noise
3	Chatter	$R_a \geq 0.6$	Significant vibration	Muffled noise

6.2. Optimization Results and Discussion

The outcomes of the turning operations, as delineated in Table 9, reveal that groups 1, 2, 3, 4, 5, 8, 11 and 12 exhibited workpiece chatter, leading to diminished processing efficiency and compromised surface finish quality. Notably, groups 8 and 11 (the combination of process parameters obtained by NSGA-III algorithm) achieved commendable processing efficiency; however, a surface roughness value of 1.354 μm and 1.273 μm was reported, indicative of significant chatter, adversely affecting the workpiece surface quality. The results show that the NSGA-III algorithm is not suitable for practical engineering problems of hard turning with double objective optimization.

Group 10, which employed process parameters refined using the original NSGA-II algorithm, when compared with group 9—whose parameters were honed with the enhanced NSGA-II algorithm—demonstrates that both sets enabled stable machining conditions. Nonetheless, group 10 presented with reduced processing efficiency and elevated surface roughness levels, underscoring the superior workpiece surface quality attainable with the process parameters derived from group 9.

Table 9. Turning results of process parameters selected by orthogonal test.

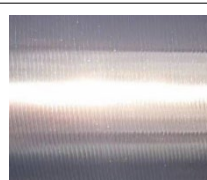
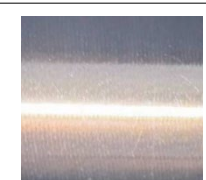
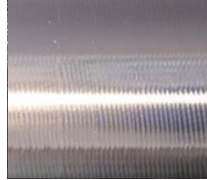
No.	1	2	3
Work-piece machined			
Surface roughness/Ra(μm)	1.352	1.486	1.845
Workpiece status	Chattering	Chattering	Chattering
Material removal rate/(mm³/min)	235.6	1178.1	1727.9
No.	4	5	6
Work-piece machined			
Surface roughness/Ra(μm)	1.174	1.574	0.958
Workpiece status	Chattering	Chattering	Transitioning
Material removal rate/(mm³/min)	779.3	1250.9	899.9

Table 9. Cont.

No.	7	8	9
Work-piece machined			
Surface roughness/ R_a (μm)	0.702	1.354	0.264
Workpiece status	Transitioning	Chattering	Stabilizing
Material removal rate/(mm ³ /min)	1885.0	2827.3	1899.9
No.	10	11	12
Work-piece machined			
Surface roughness/ R_a (μm)	0.445	1.273	1.435
Workpiece status	Stabilizing	Chattering	Chattering
Material removal rate/(mm ³ /min)	1508.0	2456.2	1982.18

In the case of keeping the processing efficiency roughly unchanged, the measured surface roughness of the workpiece stands at 0.264 μm in group 9, whereas groups 7 and 12 exhibit surface roughness values of 0.702 μm and 1.435 μm, respectively. This equates to a reduction in surface roughness of 0.438 μm and 1.171 μm for group 9 when compared to groups 7 and 12, respectively. This also proves that the performance of the improved NSGA-II algorithm is better than that of the MOEA/D algorithm.

These findings highlight that the employment of process parameters refined through the enhanced NSGA-II algorithm not only preserves processing efficiency but also significantly elevates the surface quality of the workpiece.

7. Conclusions

In this work, a study of a multi-objective process parameter optimization method for hard turning based on improved NSGA-II algorithm is proposed and shows the following conclusions:

- (1) Upon a comprehensive analysis of the structure, foundational principles, and optimization challenges inherent to the traditional NSGA-II algorithm, an enhanced variant is proposed. This refined algorithm integrates a hybrid crossover technique that amalgamates simulated binary crossover with polynomial variations, specifically addressing the original algorithm's limited convergence rates. The efficacy of this improved algorithm was rigorously tested using the benchmark ZDT series functions, both pre- and post-enhancement. The testing outcomes underscore a marked improvement in convergence speed and distribution uniformity relative to the conventional algorithm.
- (2) For the empirical segment of this study, the high-hardness alloy 20MnCrTi was selected as the subject for cylindrical hard turning experiments, utilizing PCBN cutting tools. The response variables, such as surface roughness and material removal rate, were quantified through orthogonal experimental designs. These empirical findings facilitated the derivation of a nonlinear regression equation, correlating surface roughness with the cutting parameters. Furthermore, an objective function was formulated, grounded on the theoretical underpinnings of the material removal rate.
- (3) The optimized NSGA-II algorithm was applied to the multi-objective optimization dilemma concerning the machining parameters for the high-hardness carburized steel 20MnCrTi in cylindrical turning applications. The outcomes revealed that the opti-

mized algorithm surpasses its traditional counterpart in aspects of convergence speed and precision. The machining parameters refined through this process effectively circumvent local optima, steering towards a more global optimum. Consequently, the enhanced algorithm demonstrates superior efficacy in resolving optimization issues related to cutting machining parameters.

The improved NSGA-II algorithm has certain limitations although it improves the convergence and uniformity of multi-objective optimization of machining parameters. Future work could include the following studies:

- (1) Multi-sensor fusion technology: Explore advanced multi-sensor fusion techniques to enhance machining process monitoring.
- (2) Real-time adjustment of machining parameters: Integrate optimization with machine control systems for real-time parameter adjustments.
- (3) Exploration of additional decision variables and objectives: Include more variables and new objectives to broaden the study's scope and depth.

In this study, the refined NSGA-II algorithm was applied to optimize spindle speed, cutting depth, and feed rate for improving surface roughness and material removal rate in turning carburized steel 20MnCrTi. Future research could expand its use to additional parameters such as tool wear, life, and energy consumption, and broader objectives like minimizing energy use and maximizing tool life. Moreover, the algorithm's applicability could extend beyond turning to other manufacturing processes like milling and grinding, and complex tasks such as assembly line balancing and manufacturing system design, thereby enhancing efficiency and sustainability in diverse manufacturing environments.

Author Contributions: Conceptualization, F.W. and A.W.; methodology, F.W., Z.Z. and A.W.; software, Z.Z. and A.W.; validation, Z.Z.; formal analysis, F.W., A.W. and Z.Z.; investigation, Z.Z. and A.W.; resources, F.W.; data curation, Z.Z. and A.W.; writing—original draft preparation, F.W. and Z.Z.; writing—review and editing, F.W., Z.Z. and A.W.; funding acquisition, F.W. All authors have read and agreed to the published version of the manuscript.

Funding: This work was supported in part by the National Natural Science Foundation of China under Grant No. 52175482.

Data Availability Statement: Data are contained within the article.

Conflicts of Interest: The authors declare no conflict of interest.

References

1. Hamdi, A.; Merghache, S.M. Application of artificial neural networks (ANN) and gray relational analysis (GRA) to modeling and optimization of the material ratio curve parameters when turning hard steel. *Int. J. Adv. Manuf. Technol.* **2023**, *124*, 3657–3670. [[CrossRef](#)]
2. Bober, P.; Zgodavová, K.; Čička, M.; Mihalíková, M.; Brindza, J. Predictive Quality Analytics of Surface Roughness in Turning Operation Using Polynomial and Artificial Neural Network Models. *Processes* **2024**, *12*, 206. [[CrossRef](#)]
3. Xue, H.; Li, T.; Li, J.; Zhang, Y.; Huang, S.; Li, Y.; Yang, C.; Zhang, W. Multi-Objective Optimization for Turning Process of 304 Stainless Steel Based on Dung Beetle Optimizer-Back Propagation Neural Network and Improved Particle Swarm Optimization. *J. Mater. Eng. Perform.* **2023**, *33*, 3787–3800. [[CrossRef](#)]
4. Du, Z.; Xu, W.; Wang, Z.; Zhu, X.; Wang, J.; Wang, H. Multi-objective optimization of concave radial forging process parameters based on response surface methodology and genetic algorithm. *Int. J. Adv. Manuf. Technol.* **2024**, *130*, 5025–5044. [[CrossRef](#)]
5. Gao, J.; Wang, X.; Wang, C.; Hao, Y.; Liang, X.; Li, W.; Zhao, K. Multi-objective optimization of process parameters for laser metal deposition of NiTi shape memory alloy based on neural network and genetic algorithm. *Int. J. Adv. Manuf. Technol.* **2024**, *130*, 4663–4678. [[CrossRef](#)]
6. Chu, W.-L.; Xie, M.-J.; Wu, L.-W.; Guo, Y.-S.; Yau, H.-T. The Optimization of Lathe Cutting Parameters Using a Hybrid Taguchi-Genetic Algorithm. *IEEE Access* **2020**, *8*, 169576–169584. [[CrossRef](#)]
7. Wu, P.; He, Y.; Li, Y.; He, J.; Liu, X.; Wang, Y. Multi-objective optimisation of machining process parameters using deep learning-based data-driven genetic algorithm and TOPSIS. *J. Manuf. Syst.* **2022**, *64*, 40–52. [[CrossRef](#)]
8. Qiang, Z.; Miao, X.; Wu, M.; Sawhney, R. Optimization of abrasive waterjet machining using multi-objective cuckoo search algorithm. *Int. J. Adv. Manuf. Technol.* **2018**, *99*, 1257–1266. [[CrossRef](#)]
9. Persson, H.; Bushlya, V.; Franca, L.; Zhou, J.; Ståhl, J.-E.; Lenrick, F. Performance and wear mechanisms of different PCBN tools when machining superalloy AD730. *Ceram. Int.* **2022**, *48*, 22733–22742. [[CrossRef](#)]

10. Hassan, S.; Khan, S.A.; Naveed, R.; Saleem, M.Q.; Mufti, N.A.; Farooq, M.U. Investigation on tool wear mechanisms and machining tribology of hardened DC53 steel through modified CBN tooling geometry in hard turning. *Int. J. Adv. Manuf. Technol.* **2023**, *127*, 547–564. [[CrossRef](#)]
11. Gutnichenko, O.; Nilsson, M.; Lindvall, R.; Bushlya, V.; Andersson, M. Improvement of tool utilization when hard turning with cBN tools at varying process parameters. *Wear* **2021**, *477*, 203900. [[CrossRef](#)]
12. Mo, P.; Chen, J.; Zhang, Z.; Chen, C.; Pan, X.; Xiao, L.; Feng, L. The effect of cBN volume fraction on the performance of PCBN composite. *Int. J. Refract. Met. Hard Mater.* **2021**, *100*, 105643. [[CrossRef](#)]
13. Aslantas, K.; Hasçelik, A.; Erçetin, A.; Danish, M.; Alatrushi, L.K.H.; Rubaiee, S.; Bin Mahfouz, A. Effect of cutting conditions on tool wear and wear mechanism in micro-milling of additively manufactured titanium alloy. *Tribol. Int.* **2024**, *193*, 109340. [[CrossRef](#)]
14. Tang, L.; Sun, Y.; Li, B.; Shen, J.; Meng, G. Wear performance and mechanisms of PCBN tool in dry hard turning of AISI D2 hardened steel. *Tribol. Int.* **2019**, *132*, 228–236. [[CrossRef](#)]
15. Mia, M.; Krolczyk, G.; Maruda, R.; Wojciechowski, S. Intelligent Optimization of Hard-Turning Parameters Using Evolutionary Algorithms for Smart Manufacturing. *Materials* **2019**, *12*, 879. [[CrossRef](#)] [[PubMed](#)]
16. Pourmostaghimi, V.; Zadshakoyan, M.; Badamchizadeh, M.A. Intelligent model-based optimization of cutting parameters for high quality turning of hardened AISI D2. *Artif. Intell. Eng. Des. Anal. Manuf.* **2020**, *34*, 421–429. [[CrossRef](#)]
17. de Melo, S.A.; Pereira, R.B.D.; da Silva Reis, A.F.; Lauro, C.H.; Brandão, L.C. Multi-objective evolutionary optimization of unsupervised latent variables of turning process. *Appl. Soft Comput.* **2022**, *120*, 108713. [[CrossRef](#)]
18. Hegab, H.; Salem, A.; Rahnamayan, S.; Kishawy, H.A. Analysis, modeling, and multi-objective optimization of machining Inconel 718 with nano-additives based minimum quantity coolant. *Appl. Soft Comput.* **2021**, *108*, 107416. [[CrossRef](#)]
19. Verma, S.; Pant, M.; Snasel, V. A Comprehensive Review on NSGA-II for Multi-Objective Combinatorial Optimization Problems. *IEEE Access* **2021**, *9*, 57757–57791. [[CrossRef](#)]
20. Zhang, P.; Qian, Y.; Qian, Q. Multi-objective optimization for materials design with improved NSGA-II. *Mater. Today Commun.* **2021**, *28*, 102709. [[CrossRef](#)]
21. Joshi, M.; Ghadai, R.K.; Madhu, S.; Kalita, K.; Gao, X.Z. Comparison of NSGA-II, MOALO and MODA for Multi-Objective Optimization of Micro-Machining Processes. *Materials* **2021**, *14*, 5109. [[CrossRef](#)] [[PubMed](#)]
22. Tang, W.; Jing, L.; Cao, W.; Xu, W.; Wu, X.; Liao, H. Optimization of magnetic coupling mechanism of dynamic wireless power transfer based on NSGA-II algorithm. *Sci. Rep.* **2024**, *14*, 5121. [[CrossRef](#)] [[PubMed](#)]
23. Wang, Z.; He, M.; Wu, J.; Chen, H.; Cao, Y. An improved MOEA/D for low-carbon many-objective flexible job shop scheduling problem. *Comput. Ind. Eng.* **2024**, *188*, 109926. [[CrossRef](#)]
24. Yang, X.; Li, Z.; Cao, L.; Chen, L.; Huang, Q.; Bi, G. Process optimization and quality prediction of laser aided additive manufacturing SS 420 based on RSM and WOA-Bi-LSTM. *Mater. Today Commun.* **2024**, *38*, 107882. [[CrossRef](#)]
25. Amouzgar, K.; Bandaru, S.; Andersson, T.; Ng, A.H.C. Metamodel-based multi-objective optimization of a turning process by using finite element simulation. *Eng. Optim.* **2019**, *52*, 1261–1278. [[CrossRef](#)]
26. Srinivas, N.; Deb, K. Multiobjective optimization using nondominated sorting in genetic algorithms. *Mass. Inst. Technol. Press* **1994**, *2*, 221–248. [[CrossRef](#)]
27. Deb, K.; Pratap, A.; Agarwal, S.; Meyarivan, T. A fast and elitist multiobjective genetic algorithm NSGA-II. *IEEE* **2002**, *6*, 182–197. [[CrossRef](#)]
28. Deb, K.; Jain, H. An Evolutionary Many-Objective Optimization Algorithm Using Reference-Point-Based Nondominated Sorting Approach, Part I: Solving Problems with Box Constraints. *IEEE Trans. Evol. Comput.* **2013**, *18*, 577–601. [[CrossRef](#)]
29. Fang, P.; Yang, J.; Liao, Q.; Zhong, R.Y.; Jiang, Y. Flexible Worker Allocation in Aircraft Final Assembly Line Using Multiobjective Evolutionary Algorithms. *IEEE Trans. Ind. Inform.* **2021**, *17*, 7468–7478. [[CrossRef](#)]
30. Qiao, J.; Li, F.; Yang, S.; Yang, C.; Li, W.; Gu, K. An adaptive hybrid evolutionary immune multi-objective algorithm based on uniform distribution selection. *Inf. Sci.* **2020**, *512*, 446–470. [[CrossRef](#)]
31. Darvish Damavandi, M.; Mousavi, S.M.; Safikhani, H. Pareto optimal design of swirl cooling chambers with tangential injection using CFD, GMDH-type of ANN and NSGA-II algorithm. *Int. J. Therm. Sci.* **2017**, *122*, 102–114. [[CrossRef](#)]
32. Pang, L.M.; Ishibuchi, H.; Shang, K. NSGA-II with Simple Modification Works Well on a Wide Variety of Many-Objective Problems. *IEEE Access* **2020**, *8*, 190240–190250. [[CrossRef](#)]
33. Zou, D.; Li, S.; Xuan, K.; Ouyang, H. A NSGA-II variant for the dynamic economic emission dispatch considering plug-in electric vehicles. *Comput. Ind. Eng.* **2022**, *173*, 108717. [[CrossRef](#)]
34. Zeng, G.-Q.; Chen, J.; Li, L.-M.; Chen, M.-R.; Wu, L.; Dai, Y.-X.; Zheng, C.-W. An improved multi-objective population-based extremal optimization algorithm with polynomial mutation. *Inf. Sci.* **2016**, *330*, 49–73. [[CrossRef](#)]
35. Zitzler, E.; Deb, K.; Thiele, L. Comparison of Multiobjective Evolutionary. *MIT Press* **2000**, *8*, 173–195. [[CrossRef](#)] [[PubMed](#)]
36. Schott, J.R. *Fault Tolerant Design Using Single and Multicriteria Genetic Algorithm Optimization*; Massachusetts Institute of Technology: Cambridge, MA, USA, 1995.

37. Gupta, P.; Singh, B. Ensembled local mean decomposition and genetic algorithm approach to investigate tool chatter features at higher metal removal rate. *J. Vib. Control* **2020**, *28*, 30–44. [[CrossRef](#)]
38. Patole, P.B.; Kulkarni, V.V. Optimization of Process Parameters based on Surface Roughness and Cutting Force in MQL Turning of AISI 4340 using Nano Fluid. *Mater. Today Proc.* **2018**, *5*, 104–112. [[CrossRef](#)]

Disclaimer/Publisher's Note: The statements, opinions and data contained in all publications are solely those of the individual author(s) and contributor(s) and not of MDPI and/or the editor(s). MDPI and/or the editor(s) disclaim responsibility for any injury to people or property resulting from any ideas, methods, instructions or products referred to in the content.